

NUMERICAL MODELING OF TROPOSPHERE-INDUCED GRAVITY WAVE PROPAGATION

N. M. Gavrilov and V. A. Yudin

Leningrad State University  
Leningrad-Petrodvorets, USSR

Sources of internal gravity waves (IGW) in the upper atmosphere are assumed to be meteorological processes in the troposphere. These sources are vertically and horizontally inhomogeneous and time-dependent. In order to describe the IGW propagation from such sources, a numerical solution of a system of hydrodynamical equations is required. In addition, it is necessary to take into account the influence of the altitude-latitude inhomogeneity of the temperature and wind fields on the IGW propagation as well as the processes of dissipation.

This paper proposes an algorithm for numerical modelling of the IGW propagation over a limited area from tropospheric local sources to the upper atmosphere. The algorithm takes into account all the above mentioned features. A spectral-grid method is used with the expansion of wave fields into the Fourier series over longitude. The upper limit conditions have been obtained from the requirement of a limited energy dissipation rate in an atmospheric column. The no slip (zero velocity) condition has been used at the Earth's surface.

Therefore, for the analysis of the vertical structure of steady-state oscillations, the IGW source is given in the equation for divergence as an inhomogeneous term

$$\phi = f \cdot \exp \left[ - \left( \frac{z - z_0}{d} \right)^2 \right] \exp(ik_x x - i \sigma t), \tag{1}$$

where  $f$  characterizes the source intensity,  $d$  its vertical extension,  $z_0$  is the height of the maximum,  $k_x$  and  $\sigma$  are the horizontal wave number and the IGW frequency, respectively. The values of  $z_0 = 10$  km and  $d = 5$  km have been used in the calculations, as well as the value of  $f = 10^{-11} \text{ s}^{-2}$ . The results obtained (see below) show that even this moderate value of  $f$  provides correct orders of magnitude of the IGW amplitudes in the upper atmosphere.

Wave equations are integrated over time after switching on the source (1) at a movement  $t = 0$  prior to the transition of the solution to the stationary regime. For complete stabilization of the wave oscillations regime, a time  $\Delta t \sim (60-80)\tau$  is required ( $\tau$  is the IGW period).

Fig. 1 shows profiles of the variations of wave energy dissipation  $\epsilon_w$ ; of the transmission of wave energy to the background wind  $\epsilon_b$  and the wave acceleration of the background flux  $a$  as well as the rate of dissipation of wave energy into heat  $\epsilon_\alpha$ . All curves have maxima at the heights of the lower thermosphere.

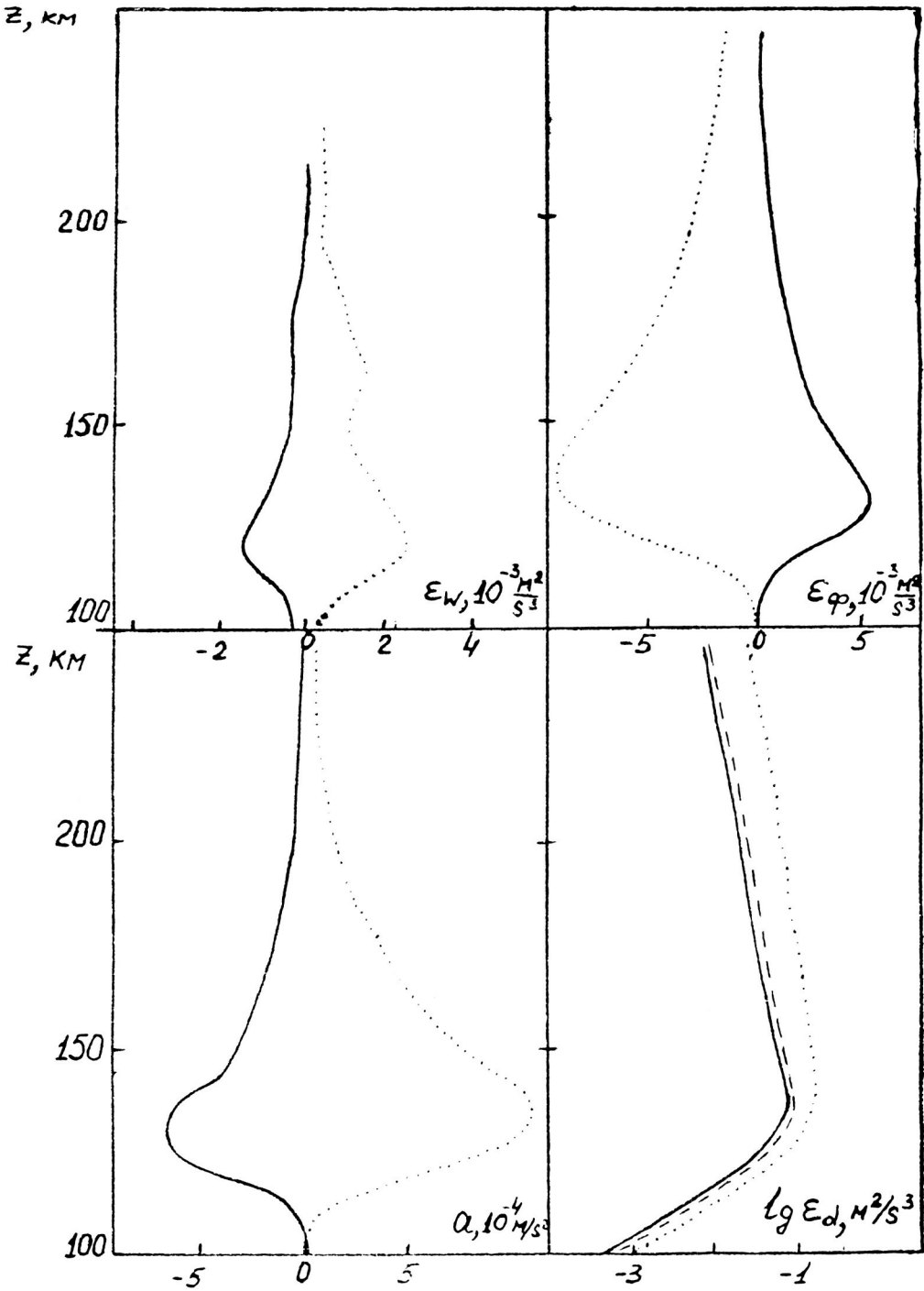


Fig. 1 Vertical Profiles of the  $\epsilon_w, \epsilon_\phi, a, lg \epsilon_d$  for January and IGW propagating to the West (solid lines) and to the East (dotted lines).

Since for the stabilization of oscillations in the atmosphere time intervals of tens and hundreds of hours are required, as was mentioned above, real meteorological sources in the atmosphere cannot, usually, remain unchanged during such long time intervals. For modelling such a source the above-mentioned inhomogeneous term in that equation for divergence has been taken as

$$\phi(x_1, z_1, t) = f \exp[-(t - t_0)^2/\tau_0^2 - (z - z_0)^2/d^2 - ik_x x], \quad (2)$$

where  $\tau_0$  is the scale of variation of the wave source in time and  $t_0$  is the time of its maximum. It can be considered that the source (2) generates a packet of IGW with the frequencies  $-\omega \leq \omega \leq \omega$  which, with a given  $k_x$ , are propagated in both directions of the axis with horizontal phase velocities  $|C_x| \leq C_m = 2\pi/(\tau_0 k_x)$ . Therefore, the values  $\tau_0$  and  $C_m$  have been used as parameters characterizing non-stationary sources. In (2) the following parameters for a tropospheric source are used:

$$f = 10^{-9} s^{-2}, \quad z_0 = 10 \text{ km}, \quad d = 5 \text{ km}$$

The results of calculations of the time variation of the integral over an atmospheric column of the wave energy  $E_{total}$  show that after the "switching on" of the source the wave energy quickly reaches its maximum values and then a slow process of attenuation begins which continues for  $(20-40) \tau_0$ . This can be accounted for by the fact that the main part of wave energy is concentrated in the tropo-strato-mesosphere and by the relatively low speed of its propagation to the thermosphere where dissipation of waves mostly takes place. The time lag of the wave energy maxima in relation to the  $\tau_0/5$  moment  $t_0$  for  $E_{total}$  is from  $\tau_0/5$  to  $\tau_0$  and for local values of  $t_0$   $E_{total}$  increases for up to  $(4-8) \tau_0$  at 100-150 km heights.

Fig. 2 shows the vertical profiles of the IGW parameters for January at various times for sources with  $\tau_0 = 6$  hrs and different  $C_m$ . Analysis of Fig. 2 shows that after a time period  $(4-8) \tau_0$  following the source function maximum a comparatively stable profile of  $E$  is formed with two maxima: in the troposphere and at the height of about 75 km. These maxima coincide with the regions of minima  $\beta H$  where  $\beta$  is the static stability parameter. The formation of the mesospheric waveguide is additionally influenced by the background wind profile which creates an increase of the wave flux  $F_z$  at the decrease of  $\lambda_z$  near the 75 km height. The formation of the waveguide leads to the lowering of the maxima of wave amplitudes and  $\epsilon_s$ ,  $\epsilon_d$  and  $a$  in Fig. 2 in comparison with the stabilized regime. Curves  $K_{lw}^w$  and  $\lambda_z$  in Fig. 2 show that in the initial period the main reflection of wave energy takes place at 80-90 km due to the effect of the temperature profile and the maximum of turbulent dissipation in the lower thermosphere. As time passes, this barrier grows more transparent and another area of increased reflection is formed near the jet stream at a height of about 50 km.

In most cases the background wind in the strato-mesosphere leads to the enhancement of the harmonics of IGW coming from the opposite direction in comparison with those propagating in the same direction, and the resulting propagation of the IGW packets is directed towards the background flux. This determines the signs of accelerations  $a$  of the background flux by

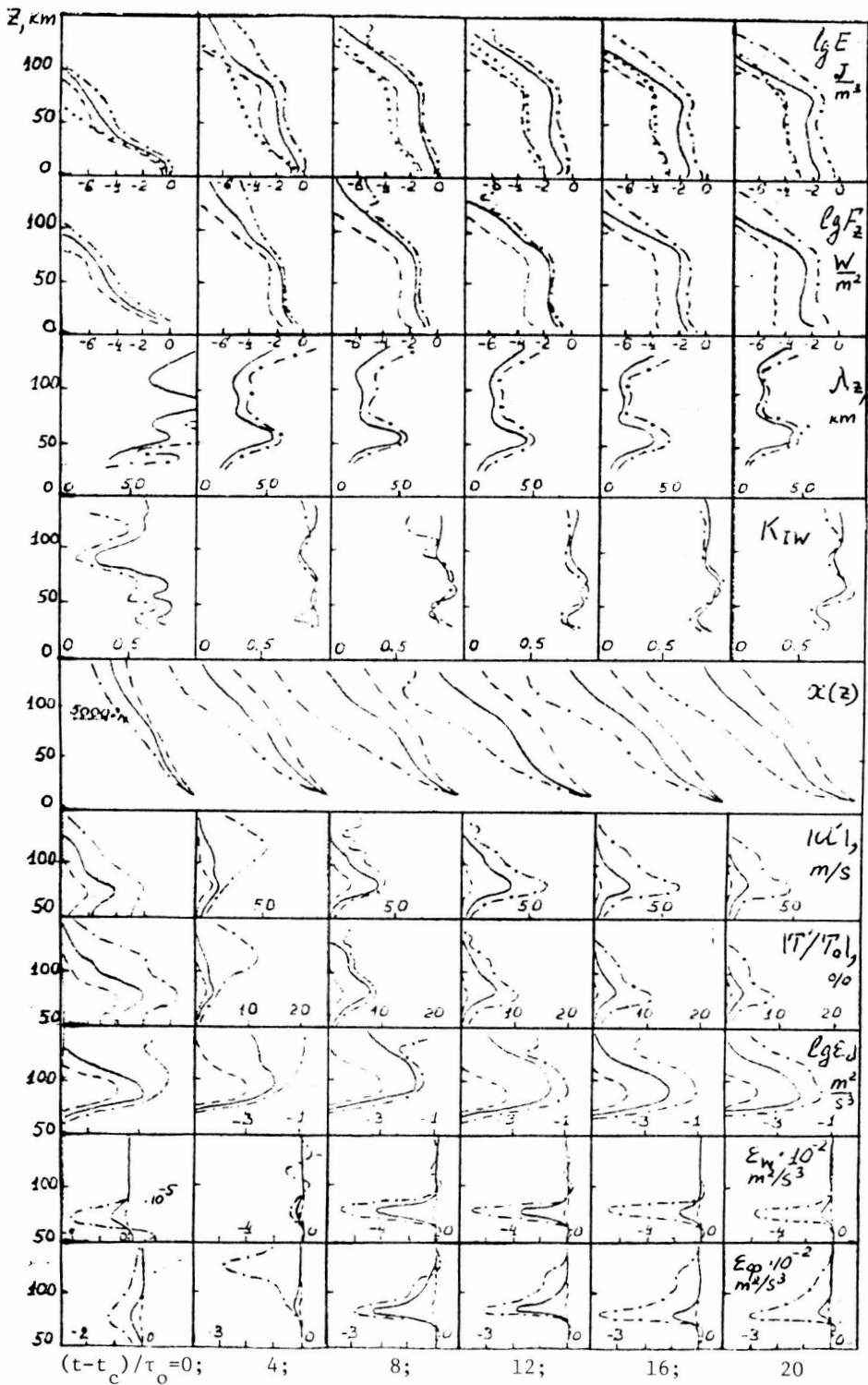


Fig. 2 Vertical profiles of IGW parameters for January at various times. Dashed, solid and dashed-dotted lines correspond to  $c_m = 90, 150$  and  $250$  mps.

waves. In winter  $a < 0$  (directed westwards); in summer, at its beginning and at heights less than 100 km,  $a > 0$  (directed eastwards) although after a time (8-12)  $\tau$  after  $t$  and above 100 km  $a < 0$  occur. According to the present-day understanding (HOLTON, 1983), the effect of IGW drag is an essential mechanism of formation of the middle atmosphere circulation. The calculations presented in this paper, according to which the filter formed by the background wind, for the most part, transmits IGW propagating from the opposite direction, account for the mechanism of appearance of dragging wave accelerations.

Fig. 3 presents the dependence on  $C_x = \sigma/k$  of the normalized wave energy  $E_{total} C_x^2 / C_x^2$  integrated over an atmospheric column, where  $C_x = 150$  mps, and on the densities of wave energy  $E$  at different height levels. The solid curves in Fig. 3 reveal, for a windless atmosphere, the resonance peaks at the values  $C_x = 310, 255$  and  $180$  mps which are very close to the values of atmospheric oscillations discussed by DIKIY (1969). The influence of the background wind leads to a bias in the resonance maxima for IGW coming from the direction opposite to the wind to  $C_x = 295, 215$  and  $125$  mps, and for IGW propagating in the direction of the wind to  $C_x = 335, 300$  and  $235$  mps, respectively. The bias of the resonance maxima in Fig. 3 is accompanied by a decrease in their values for IGW coming from the opposite direction and by an increase for those propagating in the same direction. Analysis of Fig. 3 (b through f) shows that, in the lower layers, the first resonance energy maximum prevails which corresponds to  $C_x \sim 300-315$  mps. However, as the height increases it is attenuated and at  $z \sim 100-150$  km the second resonance maximum prevails.

#### References

1. Holton, J.R., 1983, J. Atmos. Sci., 40, No. 10, 2497-2507.
2. Dikiy L.A., 1969, The Theory of The Earth's Atmospheric Oscillations, Gidrometeoizdat Publ., Leningrad, p. 196.

ORIGINAL PAGE IS  
OF POOR QUALITY

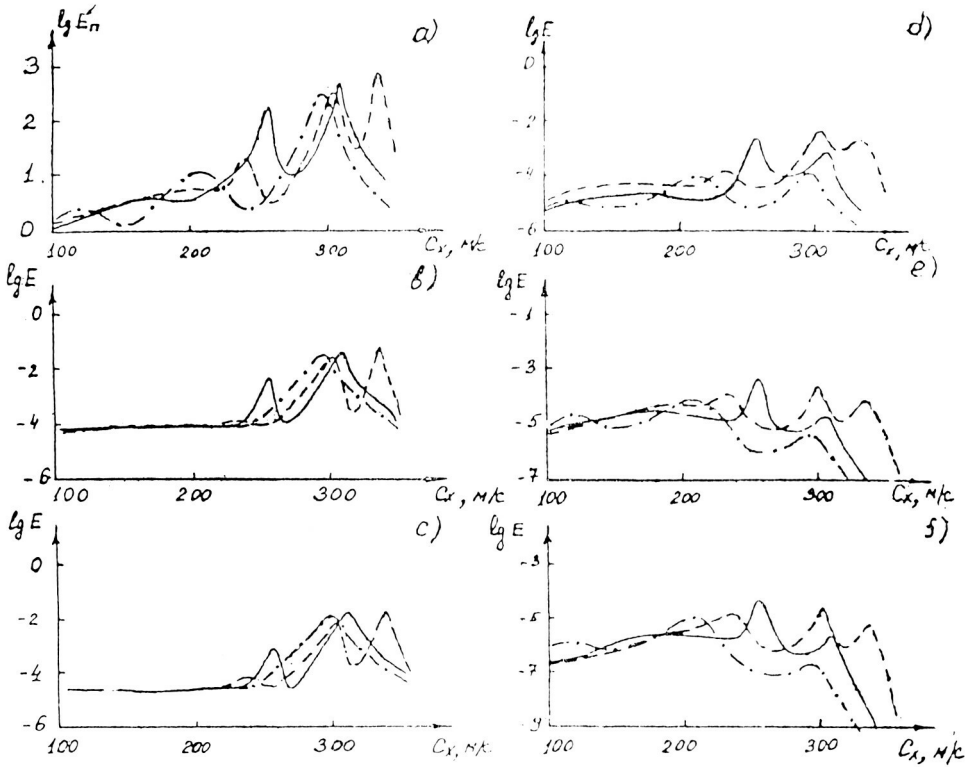


Fig. 3 Dependence on  $c_x = \sigma/k$  of  $E_n$  (frame a) and  $E$  at the height levels 1, 10, 50, 100 and 150 km, (b) through (f).